

Electronic excitation of furfural as probed by high-resolution vacuum ultraviolet spectroscopy, electron energy loss spectroscopy, and ab initio calculations

F. Ferreira da Silva, E. Lange, P. Limão-Vieira, N. C. Jones, S. V. Hoffmann, M.-J. Hubin-Franskin, J. Delwiche, M. J. Brunger, R. F. C. Neves, M. C. A. Lopes, E. M. de Oliveira, R. F. da Costa, M. T. do N. Varela, M. H. F. Bettega, F. Blanco, G. García, M. A. P. Lima, and D. B. Jones

Citation: *The Journal of Chemical Physics* **143**, 144308 (2015); doi: 10.1063/1.4932603

View online: <http://dx.doi.org/10.1063/1.4932603>

View Table of Contents: <http://scitation.aip.org/content/aip/journal/jcp/143/14?ver=pdfcov>

Published by the **AIP Publishing**

Articles you may be interested in

Electronic excitation of carbonyl sulphide (COS) by high-resolution vacuum ultraviolet photoabsorption and electron-impact spectroscopy in the energy region from 4 to 11 eV

J. Chem. Phys. **142**, 064303 (2015); 10.1063/1.4907200

Valence and ionic lowest-lying electronic states of ethyl formate as studied by high-resolution vacuum ultraviolet photoabsorption, He(I) photoelectron spectroscopy, and ab initio calculations

J. Chem. Phys. **141**, 104311 (2014); 10.1063/1.4894762

2-methyl furan: An experimental study of the excited electronic levels by electron energy loss spectroscopy, vacuum ultraviolet photoabsorption, and photoelectron spectroscopy

J. Chem. Phys. **119**, 3670 (2003); 10.1063/1.1590960

Electronic excitation and oscillator strength of ethyl bromide by vacuum ultraviolet photoabsorption and electron energy loss spectroscopy

J. Chem. Phys. **112**, 6285 (2000); 10.1063/1.481273

Electronic excitation and oscillator strength of ethyl iodide by VUV photoabsorption and electron energy loss spectroscopy

J. Chem. Phys. **110**, 10307 (1999); 10.1063/1.478964



APL Photonics is pleased to announce
Benjamin Eggleton as its Editor-in-Chief



Electronic excitation of furfural as probed by high-resolution vacuum ultraviolet spectroscopy, electron energy loss spectroscopy, and *ab initio* calculations

F. Ferreira da Silva,¹ E. Lange,¹ P. Limão-Vieira,^{1,2,a)} N. C. Jones,³ S. V. Hoffmann,³ M.-J. Hubin-Franskin,⁴ J. Delwiche,⁴ M. J. Brunger,^{2,5,a)} R. F. C. Neves,^{2,6,7} M. C. A. Lopes,⁶ E. M. de Oliveira,⁸ R. F. da Costa,^{8,9} M. T. do N. Varella,¹⁰ M. H. F. Bettega,¹¹ F. Blanco,¹² G. García,¹³ M. A. P. Lima,^{8,a)} and D. B. Jones²

¹Laboratório de Colisões Atômicas e Moleculares, CEFITEC, Departamento de Física, Faculdade de Ciências e Tecnologia, Universidade Nova de Lisboa, 2829-516 Caparica, Portugal

²School of Chemical and Physical Sciences, Flinders University, GPO Box 2100, Adelaide, South Australia 5001, Australia

³ISA, Department of Physics and Astronomy, Aarhus University, Ny Munkegade, DK-8000 Århus C, Denmark

⁴Département de Chimie, Institut de Chimie-Bât. B6C, Université de Liège, B-4000 Liège 1, Belgium

⁵Institute of Mathematical Sciences, University of Malaya, 50603 Kuala Lumpur, Malaysia

⁶Departamento de Física, Universidade Federal de Juiz de Fora, Juiz de Fora, MG, Brazil

⁷Instituto Federal do Sul de Minas Gerais, Campus Poços de Caldas, Minas Gerais, Brazil

⁸Instituto de Física “Gleb Wataghin,” Universidade Estadual de Campinas, 13083-859 Campinas, São Paulo, Brazil

⁹Centro de Ciências Naturais e Humanas, Universidade Federal do ABC, 09210-580 Santo André, São Paulo, Brazil

¹⁰Instituto de Física, Universidade de São Paulo, CP 66318, 05315-970 São Paulo, Brazil

¹¹Departamento de Física, Universidade Federal do Paraná, CP 19044, Curitiba, Paraná 81531-990, Brazil

¹²Departamento de Física Atômica, Molecular y Nuclear, Universidad Complutense de Madrid, Madrid E-28040, Spain

¹³Instituto de Física Fundamental, CSIC, Serrano 113-bis, 28006 Madrid, Spain

(Received 23 July 2015; accepted 25 September 2015; published online 13 October 2015)

The electronic spectroscopy of isolated furfural (2-furaldehyde) in the gas phase has been investigated using high-resolution photoabsorption spectroscopy in the 3.5–10.8 eV energy-range, with absolute cross section measurements derived. Electron energy loss spectra are also measured over a range of kinematical conditions. Those energy loss spectra are used to derive differential cross sections and in turn generalised oscillator strengths. These experiments are supported by *ab initio* calculations in order to assign the excited states of the neutral molecule. The good agreement between the theoretical results and the measurements allows us to provide the first quantitative assignment of the electronic state spectroscopy of furfural over an extended energy range. © 2015 AIP Publishing LLC. [<http://dx.doi.org/10.1063/1.4932603>]

I. INTRODUCTION

Furfural (2-furaldehyde), $C_5H_4O_2$, has been used extensively in the agrochemical, petroleum, plastics, and pharmaceutical industries.¹ Recent investigations have also identified furfural as a viable plant-derived biochemical alternative to petrochemicals, as a part of sustainable bio-refineries aimed at reducing pollution.^{2–5} With no direct synthetic methods of production,¹ furfural is solely produced through the thermochemical pre-treatment of biomass. While it is desirable to increase the conversion efficiency of hemicellulose into furfural, from the view point of furfural as a commodity chemical,¹ its production within some bio-refineries is undesirable, as it can inhibit enzymes responsible for up-conversion of pre-treated biomass.^{6,7} Hybrid interdisciplinary strategies represent a path forward in realising novel methods

in biomass conversion.⁸ Atmospheric pressure plasmas^{9,10} or electron-beam irradiation (EBI)^{11,12} has been identified as alternative methods for pre-treating biomass. Understanding electron-driven and photochemical processes and reaction rates, with key structural analogues of biomass, is important in understanding and potentially controlling the mechanisms that occur in plasma or EBI biomass pre-treatments with a view to promoting or eliminating particular chemical pathways.

A full understanding of the quantum chemical structure and spectroscopy of compounds produced in bio-refineries, such as furfural, is therefore essential in evaluating their role as biofuels. From a more fundamental view, a reliable quantum chemical picture is a precursor for deriving the necessary electron scattering data, and reaction rates and mechanisms, required for understanding and modelling physico-chemical processes. The importance in establishing a realistic quantum chemical picture as a basis for electron scattering calculations was highlighted in recent papers on electron scattering from phenol.^{13–15} In particular, that body of work clarified the

^{a)}Electronic addresses: plimaovieira@fct.unl.pt; michael.brunger@flinders.edu.au; and maplima@ifi.unicamp.br.

important role that multichannel coupling to excited electronic states plays in accurately describing scattering processes for complex organic targets. Establishing a detailed quantum chemical picture for furfural is therefore paramount in beginning to formulate the comprehensive electron scattering data set required to model plasma- or electron-interactions with furfural as a biomass analogue.

To begin to address these data needs, furfural has been recently studied by (e,2e) dynamical spectroscopy and He(I) photoelectron methods.¹⁶ Although several old experimental studies^{17–20} of the electronic spectrum of furfural have been reported, our knowledge of the vacuum ultraviolet (VUV) electronic state spectroscopy of furfural remains poorly quantified in a wide wavelength (λ) region. As far as we are aware, experimental information on such chemical data is mainly restricted to $\lambda \geq 222$ nm ($E \leq 5.58$ eV),²¹ and there is limited other electron scattering data for this target. Related to furfural, we have also performed photon- or electron-impact studies on the base furan structure,²² its methyl derivative,²³ 2-vinyl furan,²⁴ 2-furanomethanol (furfuryl alcohol),²⁵ azafurans²⁶ and also isoxazole,²⁷ the latter related to furan by the replacement of a CH group by a pyridine-like N atom at position 2 in the ring.

In this comprehensive study, we have performed VUV spectroscopy to identify several new features in the absorption spectrum, with special attention having been devoted to the intermediate to high energy absorption bands and to also provide reliable absolute photoabsorption cross sections. Electron energy loss spectroscopy is undertaken to clarify potential low-lying triplet states and to derive generalised oscillator strengths (GOSs). The experiments are supported by *ab initio* calculations of the vertical excitation energies and oscillator strengths for the neutral electronic transitions. The outline of our paper is as follows. In Section II, we provide a brief summary of the structure and properties of furfural, while in Section III, we present a brief discussion of the experimental methods. Subsequently in Section IV, the computational details are described. Section V is devoted to presenting and discussing the results of this study, with a comparison to other absolute photoabsorption cross sections being made where possible. Finally, some conclusions that can be drawn from this investigation are given in Section VI.

II. BRIEF SUMMARY OF THE STRUCTURE AND PROPERTIES OF FURFURAL

The molecular structure and conformations of furfural in its ground electronic state have been previously studied in the gas-phase using microwave spectroscopy, with the *trans* conformer observed to be 286 cm^{-1} (0.035 eV) more stable than the *cis* conformer.²⁸ This value is in reasonable agreement with that of $250 \pm 40\text{ cm}^{-1}$ ($0.031 \pm 0.005\text{ eV}$) as reported by Zwarich and Rabinowitz,²¹ and with the relative population weight between *trans* to *cis* of $\sim 3:1$ determined by Miller *et al.*²⁹ using the torsional frequencies in the far infrared spectrum. Vibrational analysis of the two conformers of furfural has been carried out on the basis of their IR and Raman spectra by Rogojerov *et al.*,³⁰ whereas Gandini and co-workers^{20,31} have reported on the photochemistry of furfural

in the ($\pi^* \leftarrow n$) and the lowest ($\pi^* \leftarrow \pi$) absorption bands. Finally, we note that the adiabatic and vertical energies of the lowest ionic states of furfural (ground, first-, and second-excited) have been determined by Klapstein *et al.*³² using photoelectron spectroscopy (PES).

Furfural possesses C_s symmetry in its electronic ground state for both conformers. The symmetry species available to a C_s molecule are A' and A'' , with the electronic configuration of the outermost valence orbitals of the \tilde{X}^1A' ground state calculated to be $\dots(19a')^2(20a')^2(2a'')^2(3a'')^2(21a')^2(4a'')^2$. Examination of the ground state molecular orbitals shows that the highest occupied molecular orbital (HOMO), the $4a''$ orbital, is composed of a 2p contribution from the “out-of-plane” carbonyl group oxygen atom and its coupling to the 5-member ring. This gives the $4a''$ orbital a π character. The second highest occupied molecular orbital ($21a'$, HOMO-1) is dominated by contributions from the in-plane carbonyl group oxygen 2p orbital. This orbital has typically been described as a non-bonding (n_O) orbital, although it does σ -couple to the carbon frame. The third highest occupied molecular orbital ($3a''$, HOMO-2) also displays a strong π character, arising from the ring oxygen having an out-of-plane (2p) interaction with the out-of-plane π character of the ring. Further details of these orbital characters are discussed in Ref. 16. The lowest unoccupied molecular orbital (LUMO) is mainly of anti-bonding π^* character.

The adiabatic/vertical ionisation energies (AIE/VIE), which are needed to calculate the quantum defects associated with transitions to Rydberg orbitals, have been experimentally determined in our recent study,¹⁶ using PES, to be 9.223 eV ($4a''$)⁻¹, 9.956 eV ($21a'$)⁻¹, and 10.678 eV ($3a''$)⁻¹, respectively (see also Ref. 32).

III. EXPERIMENTAL DETAILS

A. Furfural sample

The liquid sample used in the VUV and electron energy loss measurements was purchased from Sigma-Aldrich, with a stated purity of 99%. In all experiments, the sample was degassed through repeated freeze–pump–thaw cycles.

B. VUV photoabsorption

The high-resolution VUV photoabsorption spectrum (Fig. 1) was measured using the new AU-UV beam line of the ASTRID2 storage ring at Aarhus University, Denmark. The apparatus used for the measurement of photoabsorption spectra has also undergone several alterations, since that which was originally described in Eden *et al.*³³ These changes have recently been described in Ref. 34, to where the reader is referred for more detail. Briefly, the gas cell has a path length of 15.5 cm and is fitted with a heated 1 Torr baratron capacitance manometer (Setra model 774). The light enters the cell through a LiF window and exits through a MgF₂ window, the latter setting the lower limit of the detectable light to 115 nm. A small gap between the photo-multiplier tube (PMT) detector and the absorption cell is evacuated

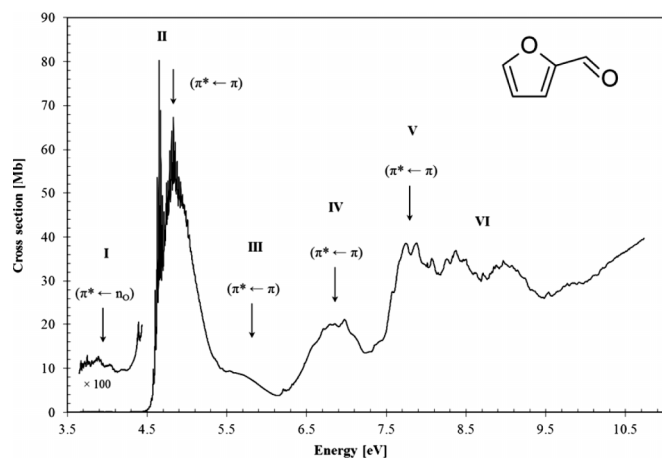


FIG. 1. High resolution VUV photoabsorption spectrum of furfural (2-furaldehyde), $C_5H_4O_2$, in the 3.5–10.8 eV photon energy range.

using a scroll pump for measurements below 200 nm. Above 200 nm air is allowed into this gap to let oxygen absorb higher orders of light (at half the chosen wavelength), which may be passing through the cell. In this way, photoabsorption measurements can be performed with spectrally pure radiation from 115 nm to 340 nm, ensuring artefact-free spectra. The synchrotron beam ring current was monitored throughout the collection of each spectrum and background scans were recorded with the cell evacuated. Absolute photoabsorption cross sections are then obtained using the Beer-Lambert attenuation law, $I_t = I_0 \exp(-n\sigma x)$, where I_t is the radiation intensity transmitted through the gas sample, I_0 is that through the evacuated cell, n is the molecular number density of the sample gas, σ is the absolute photoabsorption cross section, and x is the absorption path length (15.5 cm). The accuracy of the cross section is estimated to be $\pm 5\%$. Only when absorption by the sample is very weak ($I_0 \approx I_t$), does the error significantly increase as a percentage of the measured cross section.

To ensure that the photon data are free of any saturation effects, the absorption cross sections were measured over the pressure range 0.03–1.29 mbar, with typical attenuations of less than 30%. Finally, we note that the resolution of the instrument was 0.08 nm.

C. Electron energy loss spectroscopy

High-resolution electron energy loss spectra (EELS) [$\Delta E \sim 80$ meV (FWHM)] (see Figs. 2(a) and 2(b)) were obtained on an experimental apparatus that is housed at Flinders University. The full details of this equipment are described in Brunger and Teubner.³⁵ Briefly, a monochromated electron beam is incident on an effusive beam of furfural. The furfural vapour from a liquid reservoir ($T \sim 40$ °C) passes through a gas handling system ($T \sim 50$ °C), where it is introduced into the heated scattering chamber ($T \sim 50$ °C) through a 0.7 mm inner diameter needle. Here, the gas flow is controlled through a variable leak valve, while maintaining a chamber pressure of less than 2×10^{-5} Torr. This was selected to both limit multiple scattering events and to ensure a reasonable count rate for the experiment. An

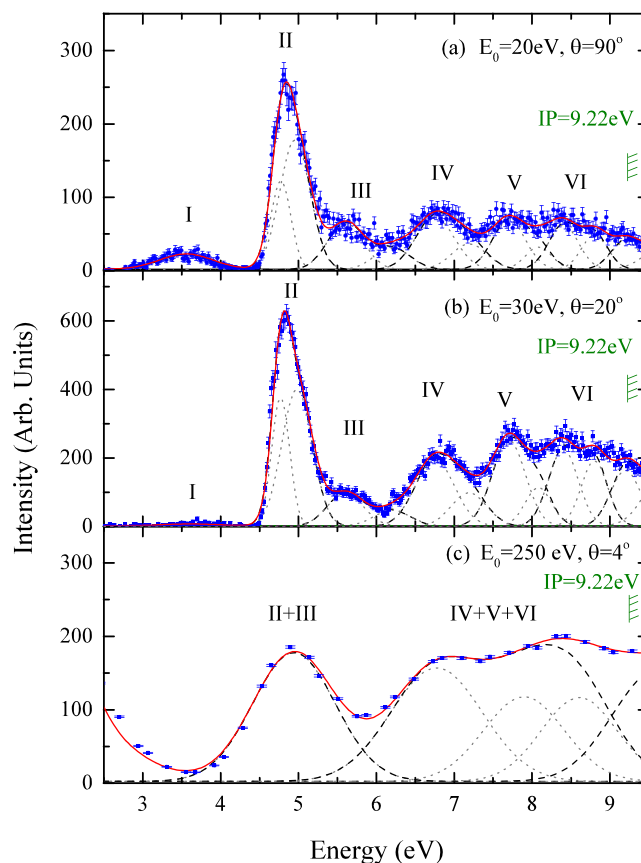


FIG. 2. Electron energy loss spectra of furfural in the 2.5–9.5 eV energy loss range at (a) 20 eV electron impact energy and a 90° scattering angle; (b) 30 eV electron impact energy and a 20° scattering angle; and (c) 250 eV impact energy and a 4° scattering angle. See text for further details.

electron analyser/detector system is mounted on a rotating table. Electrons that scatter from the furfural vapour into the acceptance cone of the analyser, at a specific angle made with reference to the incident beam direction, are energy analysed. Those electrons having the correct energy loss value pass through the analyser where they are then detected using a channel electron multiplier. In this work, we obtain energy loss spectra at fixed scattering angles of 20° and 90°, by using a multi-channel scaler to record the number of electrons detected as we continuously ramp over a range of energy loss values. Here, the energy loss is determined through,

$$E_{Loss} = E_0 - E_s, \quad (1)$$

where E_0 and E_s are, respectively, the incident and scattered electron energies.

Electron energy loss spectra of lower resolution [$\Delta E \sim 1.1$ eV (FWHM)] (a typical spectrum is shown in Fig. 2(c)) were also recorded on a different electron scattering spectrometer that was designed for measuring triple differential cross sections for electron impact ionization.³⁶ Here, the electron energy loss spectra are obtained at discrete angles in the 4°–50° range, using an un-monochromated electron beam at a higher impact energy of $E_0 = 250$ eV. This energy was chosen so that any possible triplet-state contributions to those measured energy-loss spectra were minimised. These spectra were further utilised to determine

absolute inelastic differential cross sections (DCSs) through normalising the measured inelastic to elastic scattering ratio to the elastic scattering differential cross section calculated using the Independent Atom Model–Screening Corrected Additivity Rule (IAM-SCAR) approach.^{37,38} Here, we note that in this implementation of the IAM-SCAR calculation we do not include a correction factor to preserve the optical theorem. We further note that a full discussion of elastic electron scattering from furfural is beyond the scope of this paper, rather it will be given elsewhere.³⁹ Suffice it to say that the IAM-SCAR theory is known to reliably reproduce elastic electron scattering cross sections from similar targets at higher impact energies (such as 250 eV).^{40–42} The differential scattering cross sections for excitation processes are then converted into a GOS, using the standard formula.⁴³ The properties of the GOS for dipole-allowed excitations^{43,44} allow the fitting of the GOS with the analytic functional form proposed by Vriens.⁴⁵ This functional form can be extrapolated to the optical limit, $K^2 \rightarrow 0$ a.u., to derive an experimental optical oscillator strength (OOS) for the transition. Here, K is the momentum transferred in the collision. Note that the currently employed incident electron energy ($E_0 \sim 250$ eV) is lower than that typically required to reach the optical limit.⁴⁶ However, a GOS-fitting and extrapolation approach has provided reasonable experimental OOS (to within the stated uncertainties) for a number of molecules in the recent past^{15,47–49} to energies as low as 100 eV. It is therefore useful in checking the consistency of data compiled across experiments, and scattering and quantum chemical calculations. In the absence of detailed information regarding the OOS of furfural, the implementation of our GOS approach is expected to provide a reasonable estimate of the OOS, although studies conducted at higher impact electron energies are desirable to confirm that view.

IV. COMPUTATIONAL METHODS

To assist in the interpretation of the excited state spectroscopy, we have performed a range of quantum chemical calculations. To begin, we carried out independent electronic structure calculations using the package GAMESS⁵⁰ to estimate the energy difference between the two furfural conformers. These calculations optimized the furfural geometry, with the conformer energies being obtained from the total energy calculation including a zero point energy correction. Using DFT/B3LYP/aug-cc-pVDZ, we obtained 0.0287 eV. With MP2/aug-cc-pVDZ, we obtained 0.0258 eV. The third calculation considered the geometry optimization and zero point energy at the HF/MP2/aug-cc-pVDZ level, with the total energy being calculated at the CCSD(T)/aug-cc-pVDZ level to obtain 0.0236 eV (using the scale frequency factor equal to 0.959, we obtained 0.0265 eV). The values obtained for this energy difference agree with previous calculations⁵¹ and are in reasonable accord with the experimental values^{21,28} and experimentally observed conformer populations.²⁹ The optimized geometries of both the *trans* and *cis* conformers obtained at the B3LYP/aug-cc-pVDZ level were therefore deemed suitable to use for further computations. With a view to performing extensive

electron scattering calculations within a minimal orbital basis single configuration interaction (MOB-SCI) framework, excited state calculations were performed at the full-single configuration interaction (FSCI) level. Here, a minimal basis set is required for the electron scattering calculations to become tractable.

To assess the reliability and limitations of this single-configuration interaction calculation, further time-dependent density functional theory (TD-DFT) calculations^{52,53} were performed within the Gaussian 09 package.⁵⁴ Here, we perform the TD-DFT calculations using the B3LYP functional and the aug-cc-pVDZ basis set. Note that this approach of combining FSCI and TDDFT calculations previously enabled us to provide a good quantum chemical picture of the excited electronic states of phenol,¹⁵ whilst understanding the limitation of the calculations obtained at the FSCI level. As the theoretical calculations are performed within a fixed nuclei approximation and cannot account for vibrational broadening of the experimental measurement, the present calculations are only expected to provide a qualitative description of the behaviour observed experimentally.

V. ELECTRONIC STATE SPECTROSCOPY: RESULTS AND DISCUSSION

The absolute high resolution VUV photoabsorption spectrum of furfural (2-furaldehyde) measured at room temperature is shown in Fig. 1 from 3.5 to 10.8 eV. The fine structure observed throughout the spectrum is better resolved than in previous work, enabling several Rydberg series to be assigned for the first time. It is noteworthy that the normal vibrational description may lead to some Fermi resonances, both for the valence and Rydberg excitations, making assignments particularly difficult. Our lower energy resolution electron energy loss spectra obtained under different kinematical conditions are presented in Fig. 2. These spectra are interpreted through our FSCI and TDDFT calculations which are summarised in Table I. In both the photoabsorption and energy loss spectra, the main observed absorption bands can be classified either as members of Rydberg series or as molecular valence transitions of the type ($\pi^* \leftarrow n_O$) and ($\pi^* \leftarrow \pi$).²¹ The assigned character of these transitions is further supported by our own calculations, as summarised in Table I. It is interesting to note that the first singlet excited state at both the TDDFT and FSCI levels in band I is dominated by a 21a' (HOMO-1) to 5a'' (LUMO) excitation process, as opposed to the 4a'' (HOMO) to 5a'' (LUMO) character excitation observed for the singlet transition in band II. This suggests that electron correlation plays an important role in describing excitation processes of furfural and resultantly, the excitation transition ordering. Here, we note that the correct ordering of the 21a' (HOMO-1) and 4a'' (HOMO) has been established through photoelectron spectroscopy and is supported by calculations.^{16,32} Vibronic coupling also plays an important role in the observed structure as per Tables II–V, especially in the low energy absorption band. As far as the Rydberg states are concerned, the authors are not aware of any previous results for furfural, as considered here, to have been reported in the literature. The first Rydberg members ($n = 3$)

TABLE I. Assignment of the prominent theoretically calculated singlet excited states ($f_0 > 0.010$ for bands III-VI) to the experimentally observed features in the photoabsorption and electron energy loss spectra of furfural (2-furaldehyde), $C_5H_4O_2$. For experimental band assignments, please refer to the electron energy loss spectra in Fig. 2. Also presented are the vertical excitation energies, oscillator strengths, and dominant excitation processes. Note that as the theoretical calculations utilise different orbitals, the dominant excitation processes for transitions may differ between each calculation. Triplet states are only shown for bands I and II. See text for more detail.

Expt. band	Energy (eV)	<i>trans</i> -furfural TD-DFT/aug-cc-pVDZ				<i>cis</i> -furfural TD-DFT/aug-cc-pVDZ				<i>trans</i> -furfural FSCI				<i>cis</i> -furfural FSCI			
		System	Energy (eV)	f_0	Dominant excitation	System	Energy (eV)	f_0	Dominant excitation	System	Energy (eV)	f_0	Dominant excitation	System	Energy (eV)	f_0	Dominant excitation
I	2.7-4.4	$^3A'$	2.82		$(4a'')^{-1}(5a'')$	$^3A'$	2.90		$(4a'')^{-1}(5a'')$	$^3A'$	2.60		$(4a'')^{-1}(5a'')$	$^3A'$	2.69		$(4a'')^{-1}(5a'')$
		$^3A''$	3.11		$(21a')^{-1}(5a'')$	$^3A''$	3.11		$(21a')^{-1}(5a'')$	$^3A''$	4.03		$(21a')^{-1}(7a'')$	$^3A''$	4.06		$(21a')^{-1}(7a'')$
		$^1A''$	3.65	0.000	$(21a')^{-1}(5a'')$	$^1A''$	3.65	0.000	$(21a')^{-1}(5a'')$	$^1A''$	4.72	0.001	$(21a')^{-1}(7a'')$	$^1A''$	4.76	0.000	$(21a')^{-1}(7a'')$
II	4.4-5.4	$^3A'$	4.53		$(3a'')^{-1}(5a'')$	$^3A'$	4.56		$(3a'')^{-1}(5a'')$	$^3A'$	4.46		$(4a'')^{-1}(6a'')$	$^3A'$	4.52		$(3a'')^{-1}(5a'')$
		$^1A'$	4.79	0.352	$(4a'')^{-1}(5a'')$	$^1A'$	4.90	0.351	$(4a'')^{-1}(5a'')$	$^1A'$	5.46	0.477	$(4a'')^{-1}(5a'')$	$^1A'$	5.58	0.479	$(4a'')^{-1}(5a'')$
		$^3A'$	5.01		$(4a'')^{-1}(6a'')$	$^3A'$	5.18		$(4a'')^{-1}(6a'')$	$^3A'$	5.18		$(2a'')^{-1}(7a'')$	$^3A'$	5.20		$(2a'')^{-1}(7a'')$
III	5.4-6.4	$^1A'$	5.63	0.017	$(3a'')^{-1}(5a'')$	$^1A'$	5.72	0.044	$(3a'')^{-1}(5a'')$	$^1A''$	7.28	0.034	$(4a'')^{-1}(na')$	$^1A''$	7.18	0.049	$(4a'')^{-1}(na')$
						$^1A'$	6.32	0.010	$(21a')^{-1}(22a')$	$^1A'$	7.34	0.011	$(3a'')^{-1}(5a'')$	$^1A'$	7.43	0.034	$(3a'')^{-1}(5a'')$
						$^1A''$	6.40	0.017	$(4a'')^{-1}(23a')$								
IV	6.4-7.4	$^1A'$	6.69	0.085	$(4a'')^{-1}(6a'')$	$^1A'$	6.72	0.012	$(21a')^{-1}(23a')$	$^1A'$	7.86	0.263	$(4a'')^{-1}(6a'')$	$^1A'$	8.05	0.024	$(4a'')^{-1}(7a'')$
		$^1A'$	6.84	0.028	$(21a')^{-1}(23a')$	$^1A'$	6.95	0.143	$(4a'')^{-1}(6a'')$	$^1A'$	8.09	0.034	$(4a'')^{-1}(8a'')$	$^1A'$	8.20	0.586	$(4a'')^{-1}(6a'')$
		$^1A'$	7.02	0.018	$(21a')^{-1}(24a')$	$^1A'$	7.23	0.018	$(4a'')^{-1}(7a'')$					$^1A''$	8.21	0.012	$(4a'')^{-1}(na')$
		$^1A''$	7.36	0.020	$(3a'')^{-1}(22a')$	$^1A''$	7.33	0.020	$(3a'')^{-1}(22a')$								
V	7.4-8.2	$^1A'$	7.47	0.018	$(21a')^{-1}(25a')$	$^1A'$	7.53	0.024	$(21a')^{-1}(26a')$	$^1A''$	8.70	0.039	$(3a'')^{-1}(na')$	$^1A''$	8.56	0.034	$(4a'')^{-1}(na')$
		$^1A'$	7.66	0.026	$(21a')^{-1}(26a')$	$^1A'$	8.07	0.029	$(21a')^{-1}(27a')$	$^1A'$	9.03	0.011	$(21a'')^{-1}(na')$	$^1A'$	8.92	0.019	$(21a')^{-1}(na')$
		$^1A'$	7.81	0.042		$^1A'$	8.13	0.230									
		$^1A'$	8.01	0.050	$(21a')^{-1}(27a')$												
		$^1A'$	8.09	0.106													
VI	8.2-9.0	$^1A'$	8.60	0.017	$(4a'')^{-1}(9a'')$	$^1A'$	8.38	0.016		$^1A'$	9.34	0.106	$(4a'')^{-1}(na'')$	$^1A'$	9.04	0.106	$(4a'')^{-1}(6a'')$
		$^1A'$	8.66	0.012	$(3a'')^{-1}(7a'')$	$^1A'$	8.54	0.026	$(3a'')^{-1}(7a'')$	$^1A''$	9.51	0.014	$(3a'')^{-1}(na')$	$^1A''$	9.52	0.014	$(3a'')^{-1}(na')$
		$^1A'$	8.76	0.015	$(21a')^{-1}(28a')$	$^1A'$	8.63	0.057	$(21a')^{-1}(28a')$								
						$^1A'$	8.70	0.052	$(4a'')^{-1}(9a'')$								

TABLE II. Proposed vibrational assignments in the 3.5–4.3 eV absorption band of furfural (2-furaldehyde), $C_5H_4O_2$. (w)—weak feature. (b)—broad structure (the last decimal of the energy value is given in brackets for these less-resolved features).

Energy (eV)	$\Delta\nu'_{10}$ (eV)	Assignment (this work)	Reference 18	Reference 21	Assignment (Ref. 21)
...	3.321	(0–0)
3.74(6) (w)	3.750	3.749	$1\nu'_{15} + 1\nu'_{12} + 1\nu'_5$
3.89(8) (w)	0.152	$1\nu'_{10}$
4.05(8) (b)	0.160	$2\nu'_{10}$
4.18(9) (b)	0.131	$3\nu'_{10}$

for the (ns, np, and nd \leftarrow 4a'') states converging to the ionic electronic ground state are reported with consistent δ values (Table VI), but they are weak and higher members of these series ($n > 6$) could not be proposed. Vibronic coupling is mainly due to the excitation of $\nu_{10}'(a')$, $\nu_{16/17}'(a')$, and $\nu_{19}'(a')$ quanta, corresponding to the ring stretching, ring/C—C=O deformation, and ring-CHO deformation modes, respectively.

Several other Rydberg states converging to the ionic electronic first $(21a')^{-1}$ and second $(3a'')^{-1}$ excited states of furfural have been obtained, with their origins also presented in Table VI. In addition, also for the first time, the photoabsorption spectrum was measured above 6.2 eV, thus extending the data over the lowest ionic electronic ground $(4a'')^{-1}$, first $(21a')^{-1}$, and second $(3a'')^{-1}$ excited states of furfural.

A. Valence and vibronic excitation in the range 3.5–4.3 eV (band I)

Previous UV absorption studies have reported the lowest-lying excited state of furfural at ~ 3.88 eV and assigned it to the $(\pi^* \leftarrow n_O)(\tilde{A}^1A' \leftarrow \tilde{X}^1A')$ transition,^{21,55} whereas Santhamma¹⁸ reported just a weak absorption band comprised of eleven diffuse structures with no attempt at assignment. We also note a photoemission study from Gandini *et al.*²⁰ who reported the maximum at ~ 330 nm (3.75 eV). In the present high resolution VUV spectrum, we observe a local maximum cross section of 0.13 Mb at 3.89(8) eV (Fig. 1), which is also consistent with the recent lower resolution study.⁵⁵ The origin of the band has been identified at 3.321 eV²¹ from ultraviolet absorption of furfural vapour (Table II). It should be noted that in the present measurements, the weak bands below ~ 3.74 eV are lost in the background noise, so that the (0–0) transition is not observed in the present work. The present high-resolution spectrum reveals that the fine structure is primarily attributed to excitation of the $\nu'_{10}(a')$ ring stretching mode²¹ (see Table II for the proposed assignments). The mean vibrational excitation energy of the mode is 0.148 eV from the present analysis, 0.006 eV lower than its value in the electronic ground state for *trans* furfural and 0.010 eV for the *cis*-conformer.³⁰

B. Valence and vibronic excitation in the range 4.3–5.3 eV (band II)

The valence excitation band in this energy range (Figs. 1 and 3) has been assigned to the $(\pi^* \leftarrow \pi)(\tilde{B}^1A' \leftarrow \tilde{X}^1A')$

transition in agreement with Refs. 20 and 21. The (0–0) transition has been identified at 4.602 eV by Santhamma,¹⁸ which is in very good agreement with the present value (see Table III). Gandini *et al.*²⁰ have reported the maximum at ~ 257 nm (4.82 eV). In the present high resolution VUV spectrum, we observe a local maximum cross section of 66.5 Mb at 4.831 eV (Fig. 1), in good agreement with the value of 4.835 eV from Zwarich and Rabinowitz.²¹ Gandini *et al.*,²⁰ previously reported the absence of emission in the $(\pi^* \leftarrow \pi)$ transition, which was rationalised on the basis of a fast singlet to triplet conversion involving a vibrationally excited ground-state path. The present calculations suggest that two triplet states can be found in this energy region to support this argument. Such an assertion is in agreement with the rich fine structure observed, with the clear contribution of hot-bands, from the careful analysis performed by Santhamma,¹⁸ and later explored by Zwarich and Rabinowitz.²¹ It is interesting to note that Purvis in 1910¹⁹ reported more than 30 bands in the wavelength region 253–272 nm (4.90–4.56 eV).

The origin of the band is found at 4.627 eV (see Table III), in good agreement with the 4.626 eV value from Zwarich and Rabinowitz.²¹ The excitation in this energy region is mainly due to $\nu_9'(a')$, $\nu_{15}'(a')$, $\nu_{16/17}'(a')$, $\nu_{18}'(a')$, and $\nu_{19}'(a')$ quanta, corresponding to ring stretching, ring deformation, ring/C—C=O deformation, C—C=O deformation and ring CHO stretching, and ring-CHO deformation modes, respectively.²¹ There are however several features in Table III that still remain unassigned.

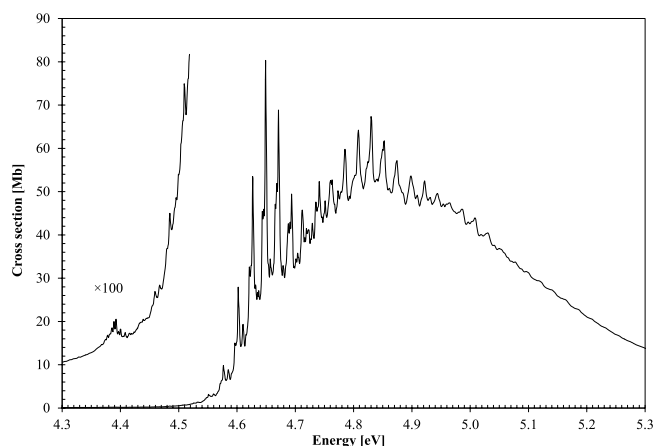


FIG. 3. High resolution VUV photoabsorption spectrum of furfural (2-furaldehyde), $C_5H_4O_2$, in the 4.3–5.3 eV photon energy range. For a detailed assignment of the features, see Table III.

TABLE III. Proposed vibrational assignments in the 4.3–5.3 eV absorption band of furfural (2-furaldehyde), C₅H₄O₂. (s)—shoulder structure. (b)—broad structure. (w)—weak feature (the last decimal of the energy value is given in brackets for these less-resolved features). ?—feature remains unassigned.

Energy (eV)	Assignment	ΔE (eV)	Energy (eV)	Assignment	ΔE (eV)
4.394	16/17 ₂ ⁰ –19 ₂ ⁰	0.025	4.752	6v' ₁₉ /2v' ₁₉ +1v' _{16/17}	0.018
4.419	16/17 ₂ ⁰ –19 ₁ ⁰	0.023	4.761	1v' ₉ +1v' ₁₅	0.020
4.437	9 ₁ ⁰ –19 ₁ ⁰	0.024	4.778	7v' ₁₉	0.026
4.442	16/17 ₂ ⁰	0.093	4.785	1v' ₉	0.158
4.461	9 ₁ ⁰	0.166	4.79(9) (s)	2v' _{16/17}	0.086
4.472	15 ₁ ⁰ –19 ₂ ⁰	0.023	4.808	1v' ₁₉ +1v' ₉	0.023
4.485	12 ₁ ⁰	0.142	4.81(9) (s)	1v' ₁₉ +2v' _{16/17}	0.020
4.495	15 ₁ ⁰ –19 ₁ ⁰	0.020	4.831	2v' ₁₉ +1v' ₉	0.023
4.515	15 ₁ ⁰	0.112	4.836	2v' ₁₉ +2v' _{16/17}	0.017
4.529	19 ₄ ⁰	0.022	4.853	2v' ₁₅ /3v' ₁₉ +1v' ₉	0.112/0.022
4.535	16/17 ₁ ⁰	0.092	4.863	3v' ₁₉ +2v' _{16/17}	0.027
4.551	19 ₃ ⁰	0.026	4.875	1v' ₉ +2v' ₁₅	0.022
4.560	?	...	4.88(6) (s)	3v' _{16/17}	0.087
4.571	18 ₁ ⁰	0.056	4.897	2v' ₉ +2v' ₁₅	0.022
4.577	19 ₂ ⁰	0.027	4.905	1v' ₁₉ +3v' _{16/17}	0.019
4.578	?	...	4.923	1v' ₁₉ +1v' ₉ +1v' ₁₅	...
4.596	?	...	4.928	2v' ₁₉ +3v' _{16/17}	0.023
4.597	?	...	4.946	2v' ₉	0.161
4.602	19 ₁ ⁰	0.025	4.958	3v' ₁₉ +3v' _{16/17}	0.030
4.617	?	...	4.96(2) (b)	3v' ₁₅ /1v' ₁₉ +2v' ₉	0.109/0.021
4.624	?	...	4.97(7) (s)	4v' _{16/17}	0.091
4.627	(0–0)	...	4.983	2v' ₁₉ +2v' ₉	0.023
4.633	?	...	5.000	1v' ₁₉ +4v' _{16/17}	0.023
4.649	1v' ₁₉	0.022	5.006	3v' ₁₉ +2v' ₉	0.022
4.650	?	...	5.01(6) (b)	1v' ₁₈ +3v' ₁₅	0.054
4.653	?	...	5.028	4v' ₁₉ +2v' ₉	0.022
4.670	2v' ₁₉	0.021	5.038	1v' ₁₉ +1v' ₉ +2v' ₁₅	...
4.671	?	...	5.05(0) (b)	4v' ₁₉ +2v' ₉	0.022
4.683	1v' ₁₈	0.056	5.07(4) (b)	4v' ₁₅ /5v' ₁₉ +2v' ₉	0.112/0.024
4.694	3v' ₁₉	0.024	5.09(6) (b)	6v' ₁₉ +2v' ₉	0.022
4.709	1v' ₁₉ +1v' ₁₈	0.026	5.11(8) (b)	7v' ₁₉ +2v' ₉	0.022
4.713	1v' _{16/17}	0.086	5.13(9) (b)	8v' ₁₉ +2v' ₉	0.021
4.714	4v' ₁₉	0.020	5.16(1) (b)	9v' ₁₉ +2v' ₉	0.022
4.734	5v' ₁₉ /1v' ₁₉ +1v' _{16/17}	0.020/0.021	5.18(9) (b)	5v' ₁₅	0.115
4.741	1v' ₁₅	0.114	5.20(4) (b,w)	1v' ₁₈ +8v' ₉ +2v' ₉	0.065

C. Valence and vibronic excitation in the range 5.3–6.4 eV (band III)

The valence band in this energy range (Figs. 1, 4, and 5) has been assigned to the ($\pi^* \leftarrow \pi$) transition in agreement with Refs. 17 and 21. The band maximum is here tentatively assigned to an energy of 5.539 eV. This value is in good agreement with Zwarich and Rabinowitch,²¹ who reported a value at ~5.58 eV. In the 5.3–6.4 eV lower energy region, we note the presence of two features at 5.416 and 5.539 eV, with an energy difference of 0.123 eV, which we assign to excitation of the v'₁₀ (a') ring stretching mode (see Fig. 5).

D. Valence and vibronic excitation in the range 6.1–7.4 eV (band IV)

The valence band in this energy range (Figs. 1, 4, and 5) is here assigned to the ($\pi^* \leftarrow \pi$) transition in agreement with Ref. 17. The (0–0) transition here has been identified at 6.18(5) eV (Table IV), in contrast to the value of 6.21 eV

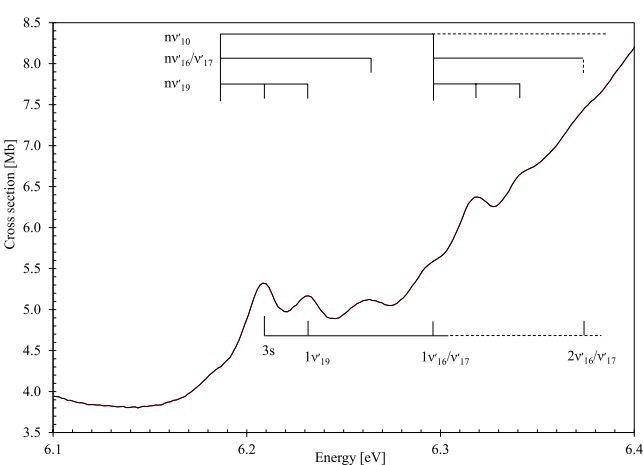


FIG. 4. High resolution VUV photoabsorption spectrum of furfural (2-furaldehyde), C₅H₄O₂, in the 6.1–6.4 eV photon energy range.

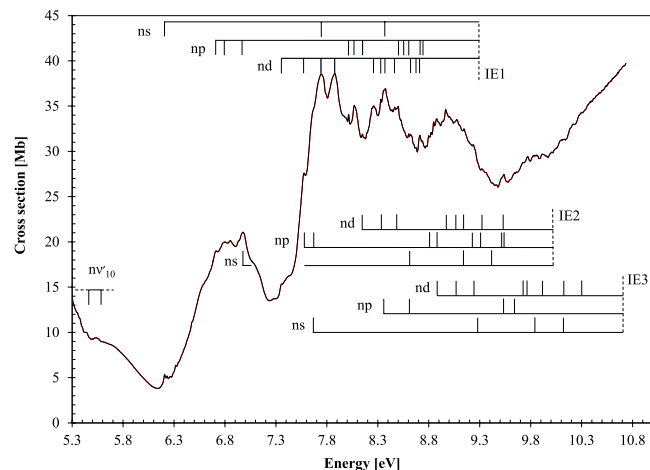


FIG. 5. High resolution VUV photoabsorption spectrum of furfural (2-furaldehyde), $C_5H_4O_2$, in the 5.3–10.8 eV photon energy range.

reported by Walsh.¹⁷ The band maximum at 6.871 eV is, however, in good agreement with the value 6.89 eV from Walsh.¹⁷ This energy region exhibits evidence for a transition to a Rydberg state assigned to $(3s \leftarrow 4a'')$ at 6.215 eV (see Section V F and Table VI) and also shows a significant number of vibrational modes being excited (Tables IV and V). These have been assigned to ν'_{19} (a') ring-CHO deformation, $\nu'_{16/17}$ (a') ring/C=C=O deformation, and ν'_{10} (a') ring stretching modes, with mean excitation energies of 0.022, 0.081, and 0.121 eV, respectively.

E. Valence and vibronic excitation in the range above 7.4 eV (bands V and VI)

From the theoretical perspective, a large number of electronic states are recovered in this energy region. These states display a high degree of mixing that makes the interpretation of this energy region particularly challenging. Within the absorption spectrum, bands have been tentatively assigned to a distinct $(\pi^* \leftarrow \pi)$ valence transition peaking at 7.895 eV (Fig. 5), in very good agreement with a TDDFT calculated state at 7.81 eV that displays strong mixing of a number of $(\pi^* \leftarrow \pi)$ transitions. There are also a number of Rydberg excitations (see Section V F and Tables V and VI). The proposed vibronic structure in this energy region is associated with Rydberg series converging to ionic electronic ground $(4a'')^{-1}$,

TABLE IV. Proposed vibrational assignments in the 6.1–6.4 eV absorption band of furfural (2-furaldehyde), $C_5H_4O_2$. (b)—broad structure. (s)—shoulder structure (the last decimal of the energy value is given in brackets for these less-resolved features).

Energy (eV)	$\Delta\nu'_{19}$ (eV)	$\Delta\nu'_{16/17}$ (eV)	$\Delta\nu'_{10}$ (eV)	Assignment
6.18(5) (b)	(0–0)
6.205	0.020	$1\nu'_{19}$
6.228	0.023	$2\nu'_{19}$
6.260	...	0.075	...	$1\nu'_{16}/1\nu'_{17}$
6.28(7) (s)	0.102	$1\nu'_{10}$
6.319	0.032	$1\nu'_{10} + 1\nu'_{19}$
6.33(9) (b)	0.020	$1\nu'_{10} + 2\nu'_{19}$
6.37(5) (b)	...	0.088	...	$1\nu'_{10} + 1\nu'_{16}/1\nu'_{17}$

TABLE V. Proposed vibrational assignments in the 6.3–10.8 eV absorption band of furfural (2-furaldehyde), $C_5H_4O_2$. (s)—shoulder structure. (b)—broad structure (the last decimal of the energy value is given in brackets for these less-resolved features).

Energy (eV)	$\Delta\nu'_{19}$ (eV)	$\Delta\nu'_{16/17}$ (eV)	$\Delta\nu'_{10}$ (eV)	$\Delta\nu'_4$ (eV)	Assignment
6.215	3s
6.228	0.013	$3s + 1\nu'_{19}$
6.28(7) (s)	...	0.072	$3s + 1\nu'_{16/17}$
6.339	0.124	...	$3s + 2\nu'_{16/17}$
6.37(5) (b)	...	0.088	$1\nu'_{10} + 1\nu'_{16}/1\nu'_{17}$
6.753	3p
6.873	0.120	...	$3p + 1\nu'_{10}$
6.783	3p'
6.92(3) (s)	0.140	...	$3p' + 1\nu'_{10}$
6.993	$3p''/3s$
7.11(3) (s)	0.120	...	$3p''/3s + 1\nu'_{10}$
7.34(5) (s)	$3p'/3s$
7.651	0.306	$3p'/3s + 1\nu'_4$
7.73(2) (b)	$3d''/4s$
7.862	0.130	...	$3d''/4s + 1\nu'_{10}$
8.017	0.366	$3p'/3s + 2\nu'_4$
8.082	0.350	$3d'' + 1\nu'_4$
8.157	$3d/4d$
8.277	0.120	...	$3d/4d + 1\nu'_{10}$
8.358	0.081	...	$3d/4d + 2\nu'_{10}$
8.486	0.128	...	$3d/4d + 3\nu'_{10}$
8.634	0.148	...	$3d/4d + 4\nu'_{10}$
8.722	$5d'''$
8.872	0.150	...	$5d''' + 1\nu'_{10}$
8.981	0.109	...	$5d''' + 2\nu'_{10}/4d$
9.089	0.108	...	$5d''' + 3\nu'_{10}$
9.127	0.255	$5d''' + 1\nu'_{10} + 1\nu'_4$
9.222	0.241	$5d''' + 2\nu'_{10} + 1\nu'_4/4d + 1\nu'_4$
9.545	6d
9.62(6) (s)	0.081	...	$6d + 1\nu'_{10}/4p'$
9.782	0.156	...	$6d + 2\nu'_{10}/4p' + 1\nu'_{10}$
9.935	0.153	...	$6d + 3\nu'_{10}/4p' + 2\nu'_{10}$

first $(21a')^{-1}$, and second $(3a'')^{-1}$ excited states of furfural that are discussed in Sec. V F. The apparent enhancement of this band due to overlap with an underlying signal suggests that these transitions are followed by dissociative processes. The proposed vibronic assignments in this energy range are listed in Table V but are not shown in Fig. 5 to avoid congestion.

F. Rydberg transitions

The VUV spectrum above 6.0 eV (Fig. 5) consists of a series of sharp and diffuse absorption features extending to the lowest ionisation energies (IEs). The experimental ionisation energy values obtained by high-resolution He(I) photoelectron spectroscopy¹⁶ are used to help tentatively assign the Rydberg series, with the proposed Rydberg structures being presented in Table VI. The peak positions, E_n , have been tested using the Rydberg formula, $E_n = E_i - R/(n - \delta)^2$, where E_i is the ionisation energy, n is the principal quantum number of the Rydberg orbital of energy E_n , R is the Rydberg constant (13.61 eV), and δ is the quantum defect resulting from the

TABLE VI. Energy value (eV), quantum defect (δ), and assignment of the Rydberg series converging to the ionic electronic ground $(4a'')^{-1}$, first $(21a')^{-1}$, and second $(3a'')^{-1}$ excited states of furfural (2-furaldehyde), $C_5H_4O_2$. (b)—broad structure. (s)—shoulder structure (the last decimal of the energy value is given in brackets for these less-resolved features).

E_n	δ	Assignment	E_n	δ	Assignment
$IE_1 = 9.223$ eV			$IE_2 = 9.956$ eV		
6.215	0.87	3s	9.222	0.69	5p
7.73(2) (b)	0.98	4s	9.53(0) (b)	0.35	6p
8.358	1.03	5s			
			7.65(1) (s)	0.57	3p'
6.753	0.66	3p	8.878	0.45	4p'
8.017	0.64	4p	9.301	0.44	5p'
8.486	0.70	5p	9.52(3) (s)	0.39	6p'
8.722	0.79	6p			
			8.157	0.25	3d
6.783	0.64	3p'	8.981	0.26	4d
8.082	0.55	4p'	9.347	0.27	5d
8.53(3) (s)	0.56	5p'	9.545	0.25	6d
8.747	0.65	6p'			
			8.358	0.08	3d'
6.993	0.53	3p''	9.050	0.12	4d'
8.157	0.43	4p''			
8.613	0.28	5p''	8.495	-0.05	3d''
			9.127	-0.05	4d''
7.34(5) (s)	0.31	3d	$IE_3 = 10.678$ eV		
8.277	0.21	4d			
8.634	0.19	5d	7.65(1) (s)	0.85	3s
			9.308	0.85	4s
7.599	0.11	3d'	9.86(4) (b)	0.91	5s
8.338	0.08	4d'	10.21(1) (b)	1.05	6s
7.73(2) (b)	-0.02	3d''	8.338	0.59	3p
8.358	0.03	4d''	9.253	0.57	4p
8.695	-0.08	5d''	8.613	0.43	3p'
7.862	-0.16	3d'''	9.62(6) (s)	0.40	4p'
8.495	-0.32	4d'''			
8.722	-0.21	5d'''	8.866	0.26	3d
			9.70(9) (s)	0.25	4d
$IE_2 = 9.956$ eV			9.089	0.07	3d'
6.993	0.86	3s	9.789	0.08	4d'
8.613	0.82	4s	10.12(1) (b)	0.06	5d'
9.133	0.93	5s	10.28(5) (s)	0.11	6d'
9.454	0.79	6s			
7.599	0.60	3p	9.253	-0.09	3d''
8.793	0.58	4p	9.89(9) (b)	-0.18	4d''

penetration of the Rydberg orbital into the core. Regarding the ionisation from the ring orbitals, the lowest energy (6.215 eV) is tentatively assigned to the Rydberg transition ($3s \leftarrow 4a''$), with a quantum defect $\delta = 0.87$, whereas the np, np', np'', nd, nd', nd'', and nd''' series are associated with the peaks at 6.753 eV ($\delta = 0.66$), 6.783 eV ($\delta = 0.64$), 6.993 eV ($\delta = 0.53$), 7.34(5) eV ($\delta = 0.31$), 7.599 eV ($\delta = 0.11$), 7.73(2) eV ($\delta = -0.02$), and 7.862 eV ($\delta = -0.16$), respectively (see Table VI). As far as the Rydberg series converging to the first ionic electronic excited state are concerned, the $n = 3$ members have been obtained for ns, np, np', nd, nd', and nd'' series with quantum defects of $\delta = 0.86$, $\delta = 0.60$, $\delta = 0.57$, $\delta = 0.25$, $\delta = 0.08$, and $\delta = -0.05$, respectively (again see Table VI).

Finally, with respect to the Rydberg series converging to the ionic electronic second excited state, a total of six series comprising excitations to ns, np, np', nd, nd', and nd'' have been obtained, the latter with members of $n = 3$ and $n = 4$. Due to the broad and structureless nature of the absorption bands, no higher order members of these Rydberg series have been proposed. We do note that the observed quantum defects are in the expected ranges for second row atoms, 0.9-1.2, ~ 0.7 , and 0-0.3 for ns, np, and nd, respectively.⁵⁶

Finally, note that the clear increase in the absorption with energy, in the range above ~ 6.3 eV, may be related to pre-dissociative or dissociative excited neutral states.

G. Electron spectroscopy

We now discuss the representative EELS (Fig. 2), obtained with the electron spectrometers at Flinders University, in more detail. First, for $E_0 = 30$ eV impact energy and a relatively small scattering angle ($\theta = 20^\circ$), Fig. 2(b), where the kinematic conditions mimic dipole scattering, the gross features of the spectrum are in excellent agreement with the measured photoabsorption spectrum. This is in spite of the energy resolution of the photoabsorption measurements being superior to that achievable in our electron scattering experiments. Second, in the EELS obtained at a lower incident electron energy ($E_0 = 20$ eV) and a large electron scattering angle ($\theta = 90^\circ$), exchange scattering allows dipole-forbidden singlet-triplet excitation processes. This produces an intense feature in band I that is much more significant than that observed in the present and previous⁵⁵ absolute photoabsorption spectra in the same energy region. The change in band I behaviour is also evident when the energy loss spectra obtained under the two different kinematical conditions are compared; Fig. 2(a) where exchange scattering is comparable in significance to dipole scattering ($E_0 = 20$ eV and $\theta = 90^\circ$) and Fig. 2(b) where dipole-scattering is preferred ($E_0 = 30$ eV and $\theta = 20^\circ$). Both the TDDFT and FSCI calculations (see Table I) suggest that two low-lying triplet states are expected in this energy region. We therefore attribute the enhanced spectral intensity observed under the scattering conditions, where exchange scattering is more prominent, to the excitation of these two triplet states. This interpretation appears to be consistent with the comment of Gandini *et al.*²⁰ that in the ($\pi^* \leftarrow n_O$) photoabsorption transition, the lack of observable fluorescence suggests a short lifetime (< 2 ns) for the singlet state, allowing an efficient intersystem crossing to the triplet manifold with a quantum yield close to unity.

Inelastic DCSs have also been derived from our energy loss spectra obtained at 250 eV impact energy that were measured over the 4° - 50° range of electron scattering angles. These DCSs are presented and tabulated in Figure 6(a) and Table VII, respectively. Also contained in this figure and table are the present IAM-SCAR elastic scattering cross sections used for normalising our experimentally determined elastic-to-inelastic ratios. Note that our energy resolution of 1.1 eV (FWHM), for the spectrum in Fig. 2(c) and others obtained with the low-resolution spectrometer, and the large number of closely located states only allow us

to de-convolve such energy loss spectra into two unique experimental features for the composite bands II + III and bands IV + V + VI. These DCSs are also converted into GOSs and fitted using the Vriens analytic formula⁴⁵ for the GOS, with the experimental data and fitted GOS also being plotted in Fig. 6(b). In the limit of K^2 goes to zero, the GOS converges to the OOS for the unresolved excitation processes. OOSs derived from the present fits to the GOSs are contained in Table VIII, where they are also compared against the summed OOSs obtained for all theoretical states recovered within each experimental band at the TDDFT and FSCI calculation levels. The resultant OOS derived for bands II + III is in good agreement with the summed OOS for the states obtained within the TDDFT calculation. The summed FSCI OOS is also in fair accord with the experimental value. This self-consistency through a combination of experiment, theoretical quantum chemistry, and IAM-SCAR scattering calculations is particularly good evidence that the excited state characterisations and elastic/inelastic electron scattering data are reliable.

For the composite experimental bands IV + V + VI, the measurement-derived oscillator strength appears to be much larger than that recovered in the TDDFT calculation. Specifically, no significantly intense states are recovered in band VI that adequately account for the prominent two features observed in the photoabsorption spectrum at ~8.5 and 9.0 eV. Here, we note that these two features have a comparable photoabsorption cross section to the feature at 7.9 eV. Thus, we expected that a significant proportion of the OOS would be missing from our summed OOS derived from the TDDFT and FSCI calculations, compared to that obtained experimentally, which is precisely what we observe in Table VIII. Also, the recovered oscillator strengths at the FSCI level, while being consistent with the TDDFT level over the sum of bands IV-VI, exhibits a different partitioning of that intensity to the individual bands. This suggests that for the future comparison of MOBS-CI inelastic differential cross sections with experimental data, it may be necessary to consider the summed intensity over the bands IV-VI.

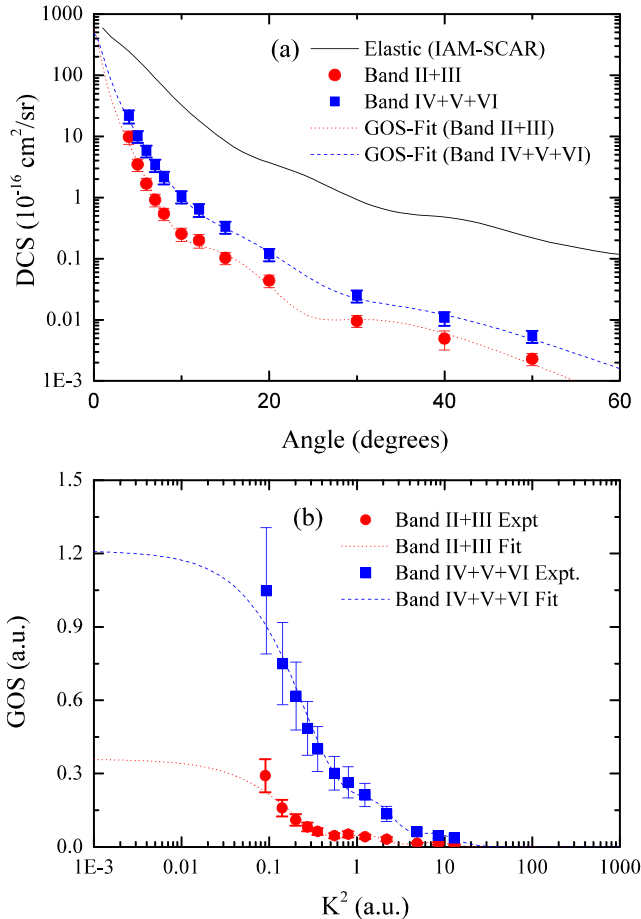


FIG. 6. (a) Elastic and inelastic differential cross sections for electron scattering from furfural at an impact energy of 250 eV; (b) generalised oscillator strengths for excitation of the II+III and IV+V+VI electronic bands of furfural. See text for further details.

H. Absolute photoabsorption cross sections and atmospheric photolysis

The present optical measurements were carried out in the pressure range 0.03-1.29 mbar and reveal no evidence

TABLE VII. Differential cross sections for elastic electron scattering and inelastic electron scattering from furfural at a 250 eV impact energy. See text for further details.

Angle (deg)	Theory	Expt.		Expt.	
	IAM-SCAR (10 ⁻¹⁶ cm ² /sr)	Band II+III (10 ⁻¹⁶ cm ² /sr)	Uncertainties (%)	Band IV+V+VI (10 ⁻¹⁶ cm ² /sr)	Uncertainties (%)
4	244.7	9.81	25	21.5	25
5	179.3	3.46	23	10.0	22
6	127.9	1.68	23	5.79	22
7	90.0	0.918	23	3.37	23
8	63.1	0.543	23	2.14	23
10	32.4	0.254	25	1.04	23
12	18.0	0.199	26	0.632	24
15	8.39	0.103	23	0.327	22
20	3.72	0.0438	23	0.118	23
30	0.921	0.0096	23	0.025	22
40	0.478	0.0049	34	0.011	25
50	0.218	0.0023	23	0.0054	23

TABLE VIII. Experimentally derived and theoretically calculated optical oscillator strengths for the composite experimental bands.

Expt. band	Energy (eV)	f_0 Expt.	Expt. band	TDDFT		FSCI	
				<i>trans</i> -furfural	<i>cis</i> -furfural	<i>trans</i> -furfural	<i>cis</i> -furfural
II+III	4.3–5.8	0.349 ± 0.025	II ($E_L \sim 4.4$ – 5.4)	0.352	0.351	0.483	0.481
			III ($E_L \sim 5.4$ – 6.4)	0.022	0.056	0.050	0.084
			Sum (II+III)	0.374	0.406	0.533	0.565
			IV ($E_L \sim 6.4$ – 7.4)	0.176	0.221	0.305	0.623
			V ($E_L \sim 7.4$ – 8.2)	0.252	0.293	0.052	0.062
IV+V+VI	5.8–9.0	1.211 ± 0.081	VI ($E_L \sim 8.2$ – 9.0) ^a	0.063	0.172	0.120	0.121
			Sum (IV+V+VI)	0.491	0.686	0.478	0.806

^aIndicates a partial sum over states recovered in the calculation. See text for further details.

for any changes in the absolute cross sections or peak energies as a function of pressure. Thus, we believe that the present spectra are free of any saturation effects. Previous UV photoabsorption cross sections of furfural are restricted to the wavelength ranges 170–200 nm (7.29–6.21 eV),¹⁷ 200–500 nm (6.20–2.48 eV),²¹ 210–370 nm (5.90–3.35 eV),⁹ 253–272 nm (4.90–4.56 eV),¹⁹ 246–280 nm (5.04–4.43 eV), and 331–369 nm (3.75–3.36 eV).¹⁸ Gandini *et al.*²⁰ reported absolute cross sections of magnitude ~ 0.11 Mb (330 nm, 3.76 eV) and ~ 76.4 Mb (257 nm, 4.82 eV), against the present respective values of 0.13 and 66.5 Mb. We believe that the observed difference, in particular at the higher energy, may be attributed to the poorer resolution of the apparatus in Gandini *et al.*²⁰ Furthermore, the general level of agreement between previous cross sections measured at the ASTRID beamline and the most precise independent data available in the literature (see Eden *et al.*⁵⁷ and references therein) suggests that the present furfural cross sections can be relied upon across the energy range studied up to 10.8 eV (see Figure 1).

The absolute photoabsorption cross sections presented in this work can be used in combination with solar actinic flux⁵⁸ measurements from the literature, to estimate the photolysis rate of furfural in the atmosphere from an altitude close to the ground to the limit of the stratopause at 50 km. Details of the programme used to achieve that are presented elsewhere.⁵⁹ Note that the quantum yield for dissociation following absorption is assumed to be unity. The reciprocal of the photolysis rate at a given altitude corresponds to the local photolysis lifetime. Photolysis lifetimes of less than 24 sunlit hr (1 day) were calculated at altitudes above 0 km. This indicates that furfural molecules can be broken up quite efficiently by UV absorption.

Rate constants for gas-phase reactions of Cl, OH, and NO₃ radicals with furfural have been recently studied by Colmenar *et al.*⁵⁵ with values of $k = 2.61 \times 10^{10}$ cm³ molecule⁻¹ s⁻¹, $k = 3.51 \times 10^{11}$ cm³ molecule⁻¹ s⁻¹, and $k = 1.20 \times 10^{12}$ cm³ molecule⁻¹ s⁻¹, respectively. Their comprehensive study has led to the conclusion that removal of furfural by reactions with OH radicals becomes more important (lifetime of 4 hr) than the UV photolysis under low solar actinic flux conditions independent of the quantum yield, whereas if the emission source also occurs during the night time, NO₃ radicals will be the main sink process (lifetime of 28 min) of such species.

I. Challenges of the theoretical electron scattering calculations

Our full-single configuration interaction calculation mentioned previously gives 53 electronic excited states (not all shown in Table I) below 10 eV and 9 states below 7 eV. The MOB-SCI calculation (obtained with selected hole-particle pairs) that will be used for further electron scattering calculations reproduces the FSCI spectrum below 7 eV but only accounts for 30 out of the possible 53 states below 10 eV. The MOB-SCI contains 63 open electronic channels (all below 26 eV), the ground state plus 31 singlet (13 below 10 eV) and 31 triplet (17 below 10 eV) states. The multichannel calculation for this system represents a big computational challenge and becomes even more demanding if we must also carry it out for both of the *trans* and *cis* geometries.

A typical furfural gas composition is made up of about 80% *trans* and 20% *cis* molecular structures. In order to understand how that could affect the theoretical study on the electron-furfural scattering problem, we carried out a preliminary calculation to obtain the elastic DCSs for energies above 15 eV for the *cis* and *trans* molecular structures. Fig. 7

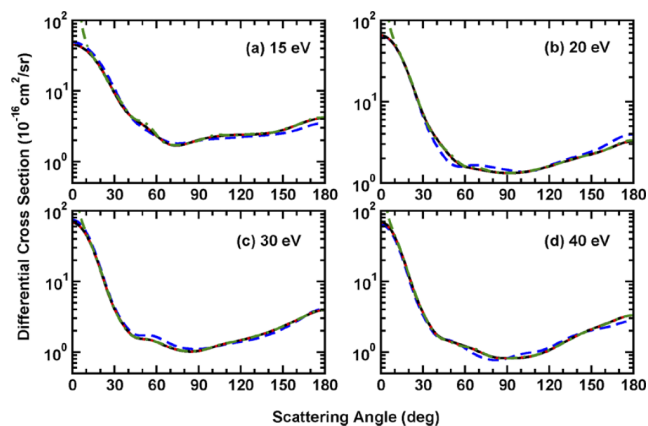


FIG. 7. Differential cross section for electron scattering from the *cis* and *trans* furfural conformers, at impact energies of 15, 20, 30, and 40 eV, as obtained with the Schwinger multichannel method with pseudopotentials at the one-channel static-exchange-plus-polarization level of approximation: *trans* structure with $L_{\text{max}} = 13$, black full line; *cis* structure with $L_{\text{max}} = 13$, blue dashed line; *trans* structure with $L_{\text{max}} = 10$, red dotted line; *trans* structure with Born-closure, green dotted-dashed line. See Ref. 60 for an explanation of the terminology used.

shows the DCS's for 15, 20, 30, and 40 eV electron impact energy obtained with the Schwinger Multichannel method with pseudopotentials⁶⁰ at the one-channel static-exchange-plus-polarization level of approximation. For details of the terminology used in this figure, please refer to Ref. 60. The results for the two isomers are very similar. This suggests that the more elaborate multichannel calculation needed to correctly describe electron scattering phenomena¹³ only needs to be undertaken for the single, most abundant, *trans* conformer.

VI. CONCLUSIONS

The present work reported the first complete study of the VUV electronic spectra of furfural and also provided the most reliable set of absolute photoabsorption cross sections available between 3.5 and 10.8 eV. Absorption bands attributed to valence and Rydberg transitions were observed, and a number of new assignments proposed on the basis of comparisons with the present *ab initio* calculations. Electron energy loss spectra measurements were also performed and yielded excellent qualitative agreement with the photoabsorption results. The EELS measurements also provided evidence for the existence of low-lying triplet states in furfural. Intermediate energy EELS measurements were also undertaken to determine generalised oscillator strengths for composite excitation bands. Optical oscillator strengths were derived from the experimental GOS and were found for bands II + III to be in excellent agreement with corresponding oscillator strengths calculated at the TDDFT level and in quite reasonable agreement with those calculated at the FSCI level for this molecule. The analysis of the observed vibronic structure in our photoabsorption spectra is generally consistent with earlier data, although the higher resolution of the present experiments has enabled us to propose assignments for Rydberg series strongly overlapping with several progressions within these bands. Finally, having quantified the electronically-excited states of furfural, it is now possible to construct a minimal-orbital-basis single configuration-interaction picture for performing high-level low-energy Schwinger multichannel electron scattering calculations. Our initial results at the 1-channel [ground electronic state] level indicated that the scattering computations need only be performed for the *trans* isomer, a significant result in terms of making our further theoretical studies tractable.³⁹ The importance of accurately describing the electronic structure in complex organic targets cannot be underestimated in electron scattering calculations, where electronic states often display strong multichannel coupling.¹³

ACKNOWLEDGMENTS

F.F.S. and P.L.V. acknowledge the Portuguese Foundation for Science and Technology (FCT-MEC) through Grant Nos. SFRH/BPD/68979/2010 and SFRH/BSAB/105792/2014, respectively, the research Grant Nos. PTDC/FIS-ATO/1832/2012 and UID/FIS/00068/2013. P.L.V. also acknowledges

his Visiting Research Fellow position at Flinders University, Adelaide, South Australia. The Patrimoine of the University of Liège, the Fonds National de la Recherche Scientifique, and the Fonds de la Recherche Fondamentale Collective of Belgium have also supported this research. E.L. and R.F.C.N. thank CNPq (Brazil) and the Science Without Borders Programme for opportunities to study abroad. The authors wish to acknowledge the beam time at the ISA synchrotron at Aarhus University, Denmark. The research leading to these results has received funding from the European Community's Seventh Framework Programme (Grant No. FP7/2007-2013) CALIPSO under Grant Agreement No. 312284. D.B.J. thanks the Australian Research Council for financial support provided through a Discovery Early Career Research Award. M.J.B. also thanks the Australian Research Council for some financial support, while M.J.B. and M.C.A.L. acknowledge the Brazilian agencies CNPq and FAPEMIG for financial support. F.B. and G.G. acknowledge partial financial support from the Spanish Ministry MINECO (Project No. FIS2012-31230) and the EU COST Action No. CM1301 (CELINA). Finally, R.F.C., M.T.do N.V., M.H.F.B., and M.A.P.L. acknowledge support from the Brazilian agency CNPq.

- ¹A. S. Mamman, J.-M. Lee, Y.-C. Kim, I. T. Hwang, N.-J. Park, Y. K. Hwang, J.-S. Chang, and J.-S. Hwang, *Biofuels, Bioprod. Biorefin.* **2**, 438 (2008).
- ²M. D'Angelantonio, S. S. Emmi, G. Poggi, and G. Beggiano, *J. Phys. Chem. A* **103**, 858 (1999).
- ³A. J. Ragauskas, C. K. Williams, B. H. Davison, G. Britovsek, J. Cairney, C. A. Eckert, W. J. Frederick, J. P. Hallett, D. J. Leak, C. L. Liotta, J. R. Mielenz, R. Murphy, R. Templer, and T. Tschaplinski, *Science* **311**, 484 (2006).
- ⁴H. Gomez Bernal, L. Bernazzani, and A. M. Raspolli Galletti, *Green Chem.* **16**, 3734 (2014).
- ⁵J.-P. Lange, E. van der Heide, J. van Buijtenen, and R. Price, *ChemSusChem* **5**, 150 (2012).
- ⁶J. D. Keating, C. Panganiban, and S. D. Mansfield, *Biotechnol. Bioeng.* **93**, 1196 (2006).
- ⁷P. Pienkos and M. Zhang, *Cellulose* **16**, 743 (2009).
- ⁸L. D. Schmidt and P. J. Dauenhauer, *Nature* **447**, 914 (2007).
- ⁹J. Amorim, C. Oliveira, J. A. Souza-Corrêa, and M. A. Ridenti, *Plasma Process. Polym.* **10**, 670 (2013).
- ¹⁰N. Schultz-Jensen, F. Leipold, H. Bindslev, and A. Thomsen, *Appl. Biochem. Biotechnol.* **163**, 558 (2011).
- ¹¹J. S. Bak, J. K. Ko, Y. H. Han, B. C. Lee, I.-G. Choi, and K. H. Kim, *Bioresour. Technol.* **100**, 1285 (2009).
- ¹²A. W. Khan, J. P. Labrie, and J. McKeown, *Biotechnol. Bioeng.* **28**, 1449 (1986).
- ¹³R. F. da Costa, E. M. de Oliveira, M. H. F. Bettega, M. T. d. N. Varella, D. B. Jones, M. J. Brunger, F. Blanco, R. Colmenares, P. Limão-Vieira, G. García, and M. A. P. Lima, *J. Chem. Phys.* **142**, 104304 (2015).
- ¹⁴R. F. C. Neves, D. B. Jones, M. C. A. Lopes, K. L. Nixon, G. B. da Silva, H. V. Duque, E. M. de Oliveira, R. F. da Costa, M. T. d. N. Varella, M. H. F. Bettega, M. A. P. Lima, K. Ratnavelu, G. García, and M. J. Brunger, *J. Chem. Phys.* **142**, 104305 (2015).
- ¹⁵D. B. Jones, G. B. da Silva, R. F. C. Neves, H. V. Duque, L. Chiari, E. M. de Oliveira, M. C. A. Lopes, R. F. da Costa, M. T. d. N. Varella, M. H. F. Bettega, M. A. P. Lima, and M. J. Brunger, *J. Chem. Phys.* **141**, 074314 (2014).
- ¹⁶D. B. Jones, E. Ali, K. L. Nixon, P. Limão-Vieira, M.-J. Hubin-Franskin, J. Delwiche, C. G. Ning, J. Colgan, A. Murray, D. H. Madison, and M. J. Brunger, "Electron- and photon-impact ionization of furfural," *J. Chem. Phys.* (submitted).
- ¹⁷A. D. Walsh, *Trans. Faraday Soc.* **42**, 62 (1946).
- ¹⁸V. Santhamma, *Proc. Natl. Acad. Sci., India, Sect. A* **22**, 256 (1956).
- ¹⁹J. E. Purvis, *J. Chem. Soc.* **97**, 1648 (1910).
- ²⁰A. Gandini, P. A. Hackett, and R. A. Back, *Can. J. Chem.* **54**, 3089 (1976).
- ²¹R. Zwarich and I. Rabinowitz, *J. Chem. Phys.* **63**, 4565 (1975).
- ²²R. F. da Costa, M. H. F. Bettega, M. A. P. Lima, M. C. A. Lopes, L. R. Hargreaves, G. Serna, and M. A. Khakoo, *Phys. Rev. A* **85**, 062706 (2012).

- ²³A. Giuliani, J. Delwiche, S. V. Hoffmann, P. Limão-Vieira, N. J. Mason, and M.-J. Hubin-Franskin, *J. Chem. Phys.* **119**, 3670 (2003).
- ²⁴A. Giuliani, I. C. Walker, J. Delwiche, S. V. Hoffmann, C. Kech, P. Limão-Vieira, N. J. Mason, and M.-J. Hubin-Franskin, *J. Chem. Phys.* **120**, 10972 (2004).
- ²⁵A. Giuliani, I. C. Walker, J. Delwiche, S. V. Hoffmann, P. Limão-Vieira, N. J. Mason, B. Heyne, M. Hoebeke, and M. J. Hubin-Franskin, *J. Chem. Phys.* **119**, 7282 (2003).
- ²⁶F. Kossoski and M. H. F. Bettega, *J. Chem. Phys.* **138**, 234311 (2013).
- ²⁷I. C. Walker, M. H. Palmer, J. Delwiche, S. V. Hoffmann, P. Limão-Vieira, N. J. Mason, M. F. Guest, M.-J. Hubin-Franskin, J. Heinesch, and A. Giuliani, *Chem. Phys.* **297**, 289 (2004).
- ²⁸R. A. Motiyenko, E. A. Alekseev, S. F. Dyubko, and F. J. Lovas, *J. Mol. Spectrosc.* **240**, 93 (2006).
- ²⁹F. A. Miller, W. G. Fateley, and R. E. Witkowski, *Spectrochim. Acta, Part A* **23**, 891 (1967).
- ³⁰M. Rogojerov, G. Keresztury, and B. Jordanov, *Spectrochim. Acta, Part A* **61**, 1661 (2005).
- ³¹A. Gandini, J. M. Parsons, and R. A. Back, *Can. J. Chem.* **54**, 3095 (1976).
- ³²D. Klapstein, C. D. MacPherson, and R. T. O'Brien, *Can. J. Chem.* **68**, 747 (1990).
- ³³S. Eden, P. Limão-Vieira, S. V. Hoffmann, and N. J. Mason, *Chem. Phys.* **323**, 313 (2006).
- ³⁴M. H. Palmer, T. Ridley, S. V. Hoffmann, N. C. Jones, M. Coreno, M. de Simone, C. Grazioli, M. Biczysko, A. Baiardi, and P. Limão-Vieira, *J. Chem. Phys.* **142**, 134302 (2015).
- ³⁵M. J. Brunger and P. J. O. Teubner, *Phys. Rev. A* **41**, 1413 (1990).
- ³⁶S. J. Cavanagh and B. Lohmann, *J. Phys. B: At., Mol. Opt. Phys.* **32**, L261 (1999).
- ³⁷F. Blanco and G. García, *J. Phys. B: At., Mol. Opt. Phys.* **42**, 145203 (2009).
- ³⁸F. Blanco and G. García, *Phys. Lett. A* **330**, 230 (2004).
- ³⁹R. F. da Costa, M. A. P. Lima, M. H. F. Bettega, E. M. de Oliveira, M. T. d. N. Varella, G. García, D. B. Jones, and M. J. Brunger, "Elastic electron collisions with furfural: an investigation on the behavior of the cross sections under the influence of multichannel coupling effects" (unpublished).
- ⁴⁰P. Paliawadana, J. Sullivan, M. Brunger, C. Winstead, V. McKoy, G. Garcia, F. Blanco, and S. Buckman, *Phys. Rev. A* **84**, 062702 (2011).
- ⁴¹L. R. Hargreaves, J. R. Brunton, A. Prajapati, M. Hoshino, F. Blanco, G. García, S. J. Buckman, and M. J. Brunger, *J. Phys. B: At., Mol. Opt. Phys.* **44**, 045207 (2011).
- ⁴²H. Kato, T. Asahina, H. Masui, M. Hoshino, H. Tanaka, H. Cho, O. Ingolfsson, F. Blanco, G. Garcia, S. J. Buckman, and M. J. Brunger, *J. Chem. Phys.* **132**, 074309 (2010).
- ⁴³E. N. Lassettre, *J. Chem. Phys.* **43**, 4479 (1965).
- ⁴⁴A. R. P. Rau and U. Fano, *Phys. Rev.* **162**, 68 (1967).
- ⁴⁵L. Vriens, *Phys. Rev.* **160**, 100 (1967).
- ⁴⁶B. R. Lewis, *Phys. Rev. A* **78**, 026701 (2008).
- ⁴⁷H. Kawahara, H. Kato, M. Hoshino, H. Tanaka, and M. J. Brunger, *Phys. Rev. A* **77**, 012713 (2008).
- ⁴⁸H. Kawahara, D. Suzuki, H. Kato, M. Hoshino, H. Tanaka, O. Ingolfsson, L. Campbell, and M. J. Brunger, *J. Chem. Phys.* **131**, 114307 (2009).
- ⁴⁹H. Kato, M. Hoshino, H. Tanaka, P. Limão-Vieira, O. Ingolfsson, L. Campbell, and M. J. Brunger, *J. Chem. Phys.* **134**, 134308 (2011).
- ⁵⁰M. W. Schmidt, K. K. Baldrige, J. A. Boatz, S. T. Elbert, M. S. Gordon, J. H. Jensen, S. Koseki, N. Matsunaga, K. A. Nguyen, S. Su, T. L. Windus, M. Dupuis, and J. A. Montgomery, *J. Comput. Chem.* **14**, 1347 (1993).
- ⁵¹K. K. Baldrige, V. Jonas, and A. D. Bain, *J. Chem. Phys.* **113**, 7519 (2000).
- ⁵²R. Bauernschmitt and R. Ahlrichs, *Chem. Phys. Lett.* **256**, 454 (1996).
- ⁵³M. E. Casida, *J. Mol. Struct.: THEOCHEM* **914**, 3 (2009).
- ⁵⁴M. J. Frisch *et al.*, GAUSSIAN 09, Revision B.01, Gaussian, Inc., Wallington, CT, USA, 2010.
- ⁵⁵I. Colmenar, S. González, E. Jiménez, P. Martín, S. Salgado, B. Cabañas, and J. Albaladejo, *Atmos. Environ.* **103**, 1 (2015).
- ⁵⁶Ed. C. Sándorfy, *The Role of Rydberg States in Spectroscopy and Photochemistry* (Kluwer Academic Publishers, Netherlands, 1999).
- ⁵⁷S. Eden, P. Limão-Vieira, S. V. Hoffmann, and N. J. Mason, *Chem. Phys.* **331**, 232 (2007).
- ⁵⁸W. B. DeMore, S. P. Sander, D. M. Golden, R. F. Hampson, M. J. Kurylo, C. J. Howard, A. R. Ravishankara, C. E. Kolb, and M. J. Molina, *Chemical Kinetics and Photochemical Data for Use in Stratospheric Modelling*, Evaluation No. 12 (JPL Publication 97-4, 1997).
- ⁵⁹P. Limão Vieira, S. Eden, P. A. Kendall, N. J. Mason, and S. V. Hoffmann, *Chem. Phys. Lett.* **364**, 535 (2002).
- ⁶⁰R. F. da Costa, M. T. d. N. Varella, M. H. F. Bettega, and M. A. P. Lima, *Eur. Phys. J. D* **69**, 159 (2015).